

ARTICLE

Investigation of structure-property-application relationships of the hydrogel-based solar vapor generator

Shudi Mao,^a An Feng,^a Stella Zhang,^a Casey Onggowarsito,^a Qian Chen,^a Dawei Su^{*b} and Qiang Fu^{*a}

Received 00th January 20xx,
Accepted 00th January 20xx

DOI: 10.1039/x0xx00000x

Without requiring any extra energy, the polymeric hydrogel based solar vapor generator (SVG) offers a promising complement to current energy-intensive desalination processes. The hydrophilic groups of polymer hydrogels can interact with water molecules through hydrogen bonding, thereby activating other adjacent water molecules to an intermediate water state, thus lowering the total enthalpy of water and making it easier to evaporate. However, there is still a knowledge gap in the structure-property relationships between hydrogel functional groups and water molecules. Here, we prepared seven hydrogels containing different functional groups, fairly compare their hydration ability and establish the relationship between the hydrophilic groups and the properties (e.g., evaporation enthalpy, electrostatic potential etc.) of the corresponding polymer hydrogels, as well as their solar evaporation performance. The resultant polyacrylamide (PAM) SVG with -NH₂ groups, standing out from the other hydrogels, shows rapid water replenishment capability, high intermediate water content of 78.2%, low equivalent water vaporization enthalpy, excellent seawater evaporation rate of 3.41 kg m⁻² h⁻¹, and excellent desalination capacity to reduce the main ion concentrations by 3-5 orders. We expect that this fundamental research could provide guidance for the development of future SVGs and ultimately contribute to the development of efficient solar vapor generation systems.

Introduction

Water is one of the most abundant resources on earth, covering three quarters of the earth's surface. However more than 97% of the earth's water is salt water in the oceans that cannot be used directly.¹ In recent decades, the demand for freshwater has been increasing due to factors such as rapid population expansion, climate change, and economic development, and has become increasingly mismatched with freshwater supply.^{2, 3} To alleviate the growing water scarcity, it is imperative to develop cost-effective, complementary technologies for desalination to extract more freshwater from the plentiful saline water resources while reducing energy consumption and environmental footprint.⁴⁻⁸ Hydrogel based solar vapor generator (SVG) is an emerging portable desalination technology that uses the heat converted from solar energy to evaporate absorbed water for freshwater acquisition. It has aroused considerable interest owing to its zero additional energy input, high solar-thermal conversion efficiency and excellent freshwater productivity.⁹⁻¹³

Compared with other raw materials, such as natural materials,¹⁴ carbon-based materials,¹⁵⁻¹⁷ coordination networks,^{18, 19} used to manufacture SVGs, polymeric hydrogels have the advantages of a straightforward fabrication process, a customizable chemical structure,

low manufacturing costs and compatibility with a variety of photo-thermal conversion materials (PTMs).²⁰⁻²² Most crucially, polymer hydrogel-based SVGs are able to evaporate water at a rate greater than the theoretical limit of 1.59 kg m⁻² h⁻¹ under one solar irradiation (1 kW m⁻²).^{23, 24} The water molecules can be divided into three categories based on how they interact with polymer chains: free water (FW), intermediate water (IW), and bound water (BW).^{25, 26} FW with solely water-water bonding has no interaction with the polymer chains, while BW with direct hydrogen bonding has the strongest interaction with polymer chains. IW is the water between BW and FW which has weakened water-water bonding, making it easier to escape from the adjacent molecules. In light of this, the IW aroused by the hydrophilic groups in the polymeric hydrogels can reduce the equivalent water vaporization enthalpy, which is the key to their high evaporation rates beyond the theoretical maximum. It's interesting to note that, in addition to polymer chains with hydrophilic groups, the recent advance in metallic λ -Ti₃O₅ by Bo Yang *et al.*,²⁷ also revealed that the excited water molecules (*i.e.* H₃O*) can be generated at the evaporation interface, which in turn facilitates the evaporation of water.

Polymer hydrogels can be made from monomers with various hydrophilic groups, such as hydroxyl group (-OH), carboxy group (-COOH), amino group (-NH₂), ester group (-C-O-C-), sulfonyl hydroxide group (-SO₃H) and others. For instance, polyvinyl alcohol (PVA) hydrogels containing numerous -OH groups initially proposed by Yu's group^{28, 29} are most often employed as SVGs due to their excellent chemical stability and low cost.³⁰⁻³⁵ While, a considerable number of studies have reported SVGs based on other hydrophilic polymer networks, such as -SO₃H groups in polystyrene sulfonates,³⁶ -NH₂ groups in polyacrylamides,^{37, 38} -C-O-C- groups in polyethylene

^a Centre for Technology in Water and Wastewater (CTWW), School of Civil and Environmental Engineering, University of Technology Sydney, Ultimo, 2007, Australia. Email: qiang.fu@uts.edu.au

^b School of Mathematical and Physical Sciences, University of Technology Sydney, Ultimo, 2007, Australia. E-mail: Dawei.Su@uts.edu.au

Electronic Supplementary Information (ESI) available: [details of any supplementary information available should be included here]. See DOI: 10.1039/x0xx00000x

glycols^{39, 40}. Unfortunately, these studies have overlooked the structure-property-application relationship of hydrogel-based SVG systems. We saw this is an opportunity to investigate the overall performance of SVGs from a materials chemistry perspective, and hope that this research will fill the knowledge gap and further provide more guidance for the development of next generation SVG.

Here, we prepared a series of polymer hydrogels with various functional groups by free radical cross-linking, systematically investigated the interactions between water molecules and different hydrophilic groups in the hydrogels, and compared their overall SVG performance. Specifically, monomers used included 2-acrylamido-2-methyl-1-propanesulfonic acid (AMPSA) with $-\text{SO}_3\text{H}$ group, acrylic acid (AA) with $-\text{COOH}$ group, 2-hydroxyethyl acrylate (HEA) with $-\text{OH}$ group, poly(ethylene glycol) diacrylate (PEGDA) with $-\text{C}-\text{O}-\text{C}-$ group, *N,N*-dimethylacrylamide (DMA) with dimethylamino groups ($-\text{N}(\text{CH}_3)_2$), acrylamide (AM) with $-\text{NH}_2$ group, and [2-(acryloyloxy)ethyl]trimethylammonium chloride (AETAC) with quaternary ammonium groups ($-\text{N}^+(\text{CH}_3)_3\text{Cl}^-$). The corresponding

hydrogels were then fabricated by free radical cross-linking induced by ammonium persulfate (APS) with the addition of a trace amount of graphene oxide as PTM. Due to the different preference of hydrophilic groups for water molecules, the highly charged polymer chains with $-\text{SO}_3\text{H}$ or $-\text{N}^+(\text{CH}_3)_3\text{Cl}^-$ group have stronger interactions with water molecules and therefore show the lowest solar evaporation performance. While, the solar evaporation performance of neutral polymer chain hydrogels were $-\text{NH}_2 > -\text{N}(\text{CH}_3)_2 > -\text{C}-\text{O}-\text{C}- > -\text{OH} > -\text{COOH}$ in descending order due to the gradual decrease in the IW content and the increase in the hydrogen bonding energy and equivalent water evaporation enthalpy.

Results and discussion

In this work, seven hydrogels with 15 wt% of polymer contents (the molar ratio of [monomer]:[crosslinker] = 9:1) and 1 wt% of photothermal materials were fabricated through the same free radical cross-linking and freeze-thawing process for fair comparison (Figure 1a).

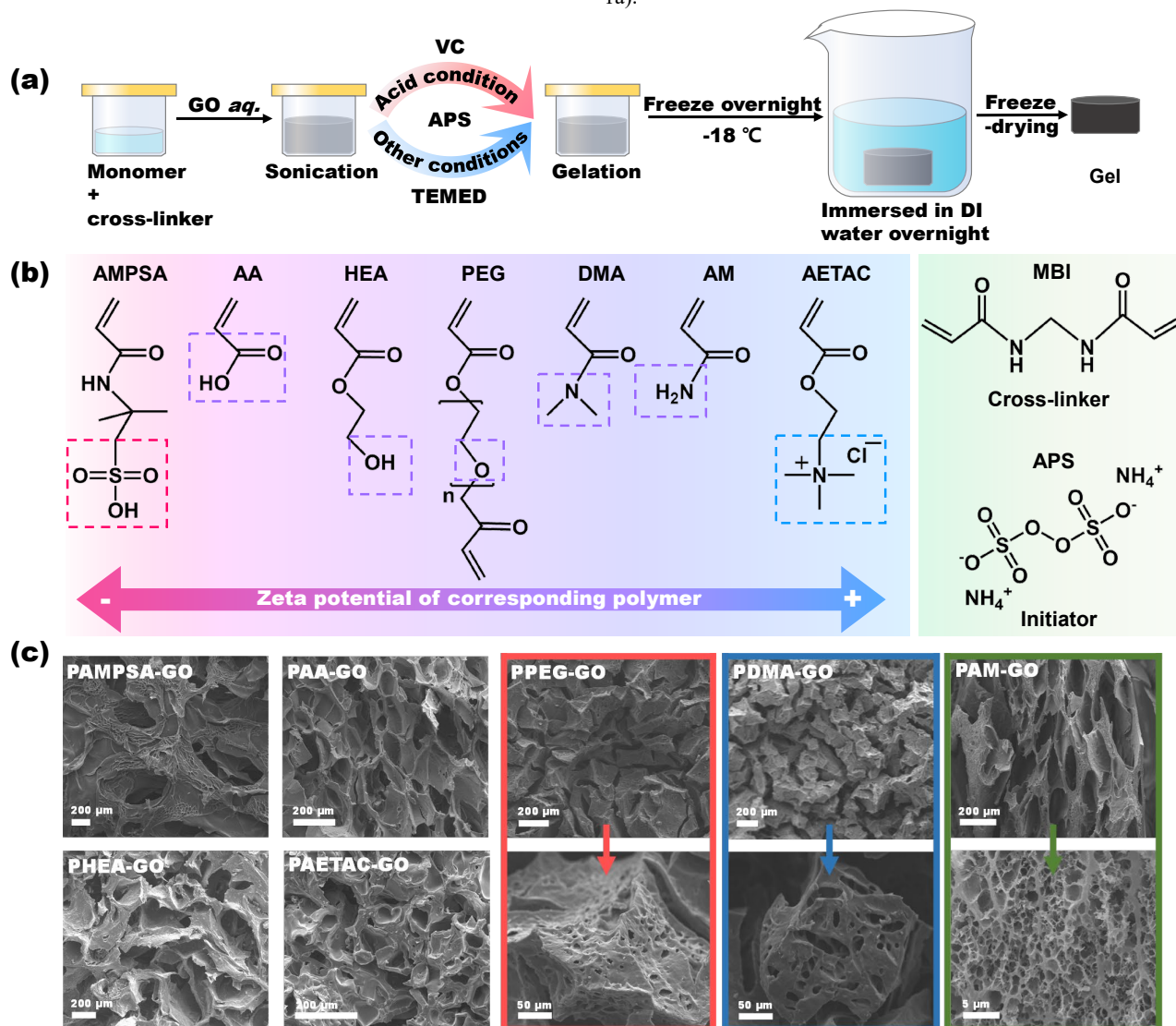


Figure 1. (a) Schematic illustration of the preparation of the hydrogel SVGs. (b) Chemical structures of the monomers, cross-linker and initiator. (c) Cross-section SEM figures of the fabricated hydrogels: PAMPSA-GO, PAA-GO, PHEA-GO, PPEG-GO, PDMA-GO, PAM-GO and PAETAC-GO. Among them, PPEG-GO, PDMA-GO and PAM-GO have micropores distribution on their macroporous walls.

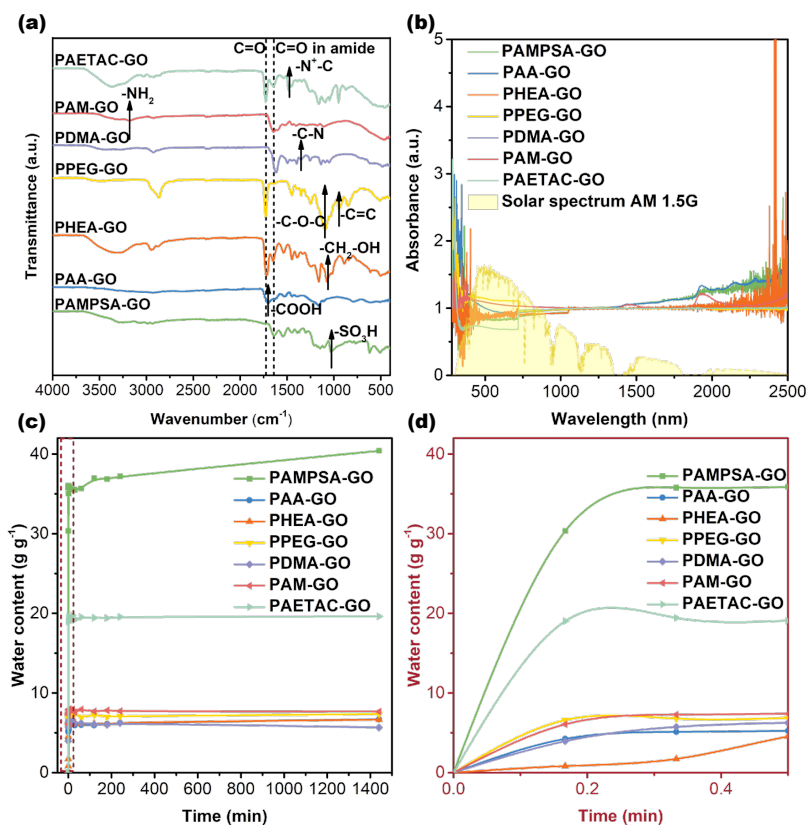


Figure 2. (a) FT-IR spectra of PAMPSA-GO, PAA-GO, PHEA-GO, PPEG-GO, PDMA-GO, PAM-GO and PAETAC-GO. (b) UV-vis-NIR spectra of all the hydrogels and the solar spectrum (AM 1.5 G) with normalised spectral solar irradiance density (the light-yellow region) spanning the wavelength range of 280-2,500 nm. The water absorbed in the gel per gram of the dried gel plotted versus the absorption time within (c) 24 hours and (d) 30 s.

Specifically, seven monomers with various hydrophilic groups were dissolved in DI water in seven different vials, including AMPSA with $-\text{SO}_3\text{H}$ groups, AA with $-\text{COOH}$ groups, HEA with $-\text{OH}$ groups, PEG with $-\text{C}-\text{O}-\text{C}-$ groups, DMA with $-\text{N}(\text{CH}_3)_2$ groups, AM with $-\text{NH}_2$ groups, and AETAC with $-\text{N}^+(\text{CH}_3)_3\text{Cl}^-$ groups (Figure 1b). *N,N'*-methylenebis(acrylamide) (MBI) was added into seven vials as the cross-linker, except for the PEGDA vial, which could cross-link with itself. These vials were subsequently infused with the same amount of graphene oxide (GO) dispersion (photothermal material, the material to transfer solar energy into thermal energy), followed by 5 minutes of sonication. Thereafter, APS (initiator) together with appropriate catalyst were added to trigger the gelation process. After 5 minutes of gelation at a steady state, the obtained hydrogels were frozen at -20°C and thawed in DI water to facilitate the internal pores formation.⁴¹ These hydrogels were freeze-dried before characterization and water evaporation tests. The fabricated gels were denoted as polymer-GO.

We also prepared seven polymers by omitting the cross-linker and tested the zeta potential of the corresponding polymers. The average value from three times of zeta potential testing for PAMPSA, PAA,

PHEA, PPEG, PDMA, PAM, and PAETAC polymers was -82.6 , -11.3 , -1.9 , -1.8 , 0.6 , 3.3 and 68.4 mV, respectively. The high charge of PAMPSA and PAETAC were attributed to the $-\text{SO}_3\text{H}$ or $-\text{N}^+(\text{CH}_3)_3\text{Cl}^-$ groups, respectively. While the charges of other polymers were close to zero with a slightly gradual increasing trend.

The successful fabrication of hydrogel SVGs was firstly evidenced by their cross-section scanning electron microscope (SEM) figures (Figure 1c). With the same freeze-thawing process, all of the hydrogels presented numerous uniformly distributed interconnected interior channels for rapid water transport. Among them, PPEG-GO, PDMA-GO and PAM-GO had a hierarchical porous structure with micropores embedded in the microporous walls, allowing for adequate hydration effect with the water molecules. PAM-GO, in particular, exhibited more open macropores and thinner walls with denser and smaller micropores than the other two hydrogels, suggesting higher capacity to water transport and absorption. However, the correlation between the pore structure and the SVG performance is still a knowledge gap to address, as different literature

illustrated seemingly contradictory conclusions. For example, a previous literature demonstrated that increasing pore size can ensure rapid water transport for higher evaporation rate,⁴² while another study proved that narrow channels can provide stronger capillary effect for better SVG performance.⁴³ Therefore, in this work we used a quantifiable characteristic mostly influenced by the pore architectures, *i.e.* the water uptaking speed mentioned below, to assess the SVG potential of hydrogels.

To confirm the chemical structure of the synthesized hydrogels, Fourier-Transform Infrared (FT-IR) spectra has been performed (Figure 2a). With the exception of PAMPSA-GO, PDMA-GO, and PAM-GO, which contain -C(=O)N- in the amide groups (1,640 cm⁻¹), all other hydrogels show a peak at 1725 cm⁻¹, which is attributed to the vibration of the carbonyl group (C=O). The characteristic absorption signals of all the hydrogels hydrophilic groups can be vividly distinguished from the spectra, including the peak observed at 1,030 cm⁻¹ representing for the -SO₃H groups of PAMPSA-GO, the peak observed at 1,700 cm⁻¹ representing for the -COOH groups of PAA-GO, the peak observed at 1,050 cm⁻¹ representing for the -OH groups of PHEA-GO, the peak observed at 1,102 cm⁻¹ representing for the -C-O-C- groups of PPEG-GO, the peak observed at 1,350 cm⁻¹ representing for the -C-N bonding of PDMA-GO, the peak observed at 3,180 cm⁻¹ representing for the -NH₂ groups of PAM-GO, and the peak observed at 1,480 cm⁻¹ representing for the -N⁺-C bonding of PAETAC-GO. In all, the FT-IR results demonstrated the successful synthesis of seven hydrogels.

We then conducted the UV-visible-NIR measurements to determine the light absorption ability of the hydrogels, which is essential for SVG application (Figure 2b). With the same amounts of GO incorporated into the hydrogels as PTM, all the hydrogels exhibit extensive light absorption across the whole solar spectrum (from 280 to 2,500 nm), indicating their similar light absorption capability.

Rapid water uptaking capacity can ensure sufficient water replenishment to the evaporation interface for continuous solar vapor generation. For comparison, we dropped the dried gels into DI water, weighed the hydrogels' weight over time (m_t), and calculated the absorbed water content via equation (1):

$$Q = (m_t - m_0)/m_0 \quad \text{Eq. (1)}$$

where m_0 is the dried gel's weight. As shown in Figure 3c, all the hydrogels can reach a saturated state within 30 seconds, suggesting rapid water uptaking capacity. Owing to the high charges of PAMPSA and PAETAC polymer chains, the saturated water content of corresponding hydrogels is much higher than other hydrogels. However, the absorption of too much water in the hydrogel can lead to heat loss to the bulk water and reduce solar vapor generation performance. While the saturated water content of other neutral polymer hydrogels is around 7 g g⁻¹. Among them, the PPEG-GO, PDMA-GO and PAM-GO exhibited slightly higher saturated water content as well as faster water uptaking rate (Figure 3d), which can be attributed to their hierarchical porous structure. Of particular note, the more porous PAM-GO and PPEG-GO hydrogels showed similar water uptake behaviour, but the PAM-GO hydrogel's SVG performance was better. This result can be attributed to the different effects of different pendant groups on water molecules.

To study the interaction between hydrophilic groups and the water molecules, we first used *Avogadro* software to simulate the chemical potential of weakened hydrogen bonding of IW based on Merck Molecular Force Field 94 (mmff94) (Figure S2-3 and Table S1). The strongly polarized electron-rich and -poor zones in the electrostatic potential maps (Figure S2) guarantee the hydrophilicity of these hydrogels.⁴⁴ For a simplified and straightforward comparison, we introduced one water molecule to a specific polymer repeating unit as the BW, and then attached the second water molecule to the first as the IW. We subsequently simulated the energy difference E_{hyd} of a single polymer repeating unit before and after an IW escaping. Thus, the E_{hyd} value is arguably to reflect the difficulty of freeing the attracted IW from hydrogen bonding with the BW on different functional groups. The simulated E_{hyd} values for PAMPSA-GO, PAA-GO, PHEA-GO, PPEG-GO, PDMA-GO, PAM-GO and PAETAC-GO are 23.94, 17.17, 12.51, 9.64, 8.96, 6.68, and 26.78 kJ mol⁻¹, respectively. The E_{hyd} values towards different groups can be ranked from low to high: -NH₂ < -N(CH₃)₂ < -C-O-C < -OH < -COOH < -SO₃H < -N⁺(CH₃)₃Cl.

The IW content was then determined by Raman measurements (Figures 3a-3h). The characteristic peaks of free water with four hydrogen bonds are located around 3,233 cm⁻¹ and 3,401 cm⁻¹ and were labeled in pink, while the characteristic peaks of intermediate water with weaken bonds are located near 3,514 cm⁻¹ and 3,630 cm⁻¹ and were indicated in light blue.^{28, 29} The ratio of the intermediate water to the sum of intermediate water and free water [IW:(IW+FW)] derived from the integrated areas under the fitting peaks is commonly used to indicate the intermediate water content. As seen, PAMPSA-GO and PAETAC-GO showed a relatively low IW content of 0.559 and 0.538, respectively, compared to the other neutral polymer-based hydrogels. Although the hydrogels based on highly charged polymers can adsorb large amounts of water, resulting in a high swelling ratio, most of them are FW. For neutral polymer hydrogels, PAM-GO exhibits the highest IW content of 0.782, followed by PDMA-GO, PPEG-GO, PHEA-GO, and PAA-GO. To summarize, the IW content in hydrogels can be ranked from high to low as -NH₂ > -N(CH₃)₂ > -C-O-C- > -OH > -COOH > -SO₃H > -N⁺(CH₃)₃Cl. Interestingly, this is the opposite of the orderliness of hydrogels E_{hyd} .

After thoroughly investigating the interactions between polymer hydrogels and water molecules absorbed, we used a home-made setup (Figure 4a) to determine their SVG performance under one sun. To ensure that the testing hydrogel can perpendicularly float on the water surface, it was fixed in the middle of a polythene (EPE) foam. For minimizing the impact of additional variables, a parafilm was used to seal minute gaps between the foam edge and the container wall to prevent any bulk water evaporation, while a thick EPE foam was added beneath the container to prevent the heat transfer to the mass balance. A portable infrared camera was used to take thermal images (Figure 4b and S4) to record the evaporation surface temperature and the bulk water temperature during the SVG process. As shown in Figure 4c, all hydrogel surfaces could reach a dynamic equilibrium temperature of 37-39 °C after *approx.* 20 minutes irradiation. The bulk water temperatures (around 30 °C) were significantly lower than the surface temperatures, suggesting the thermal confining capability of the polymeric hydrogel. The PAMPSA-GO and PAETAC-GO

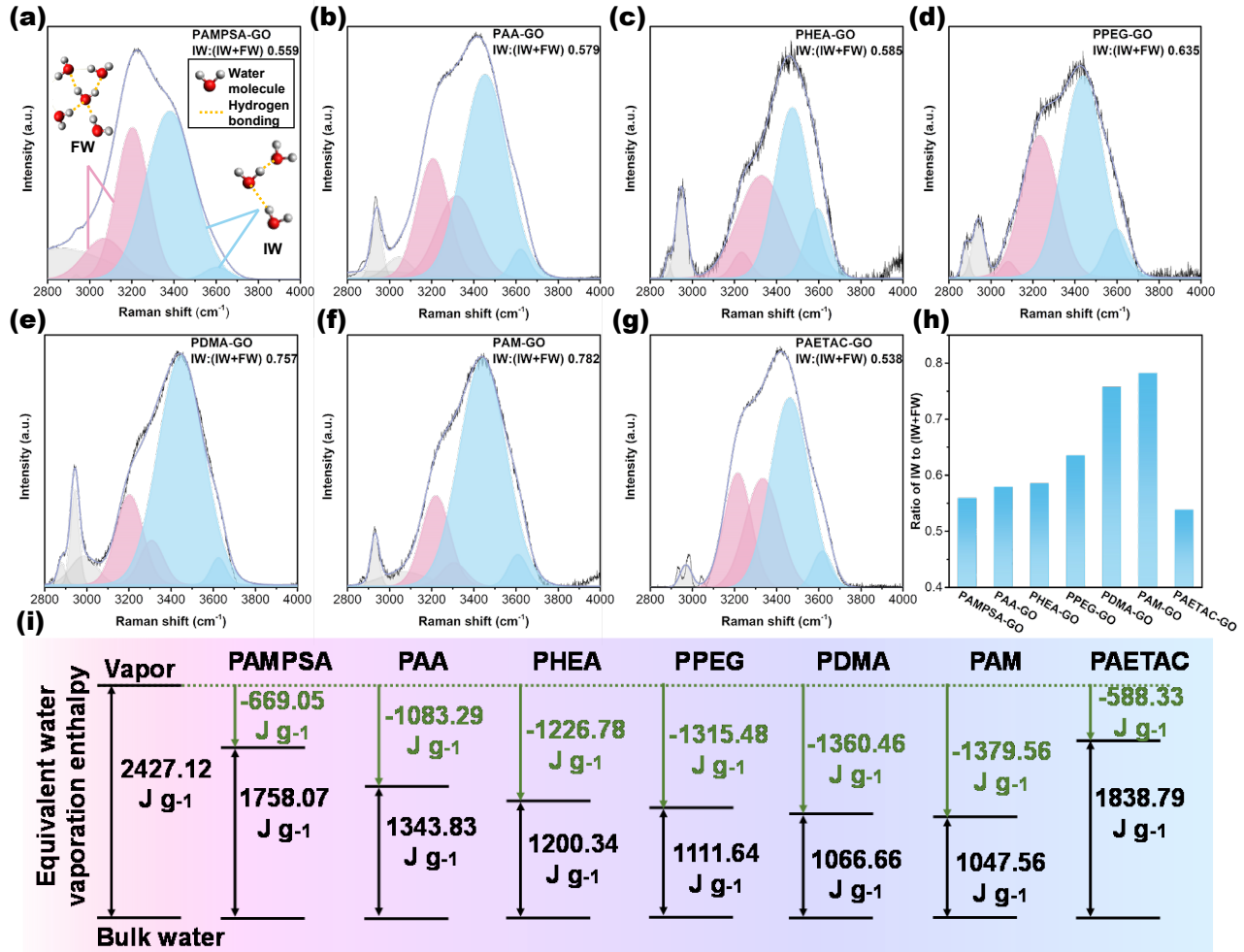


Figure 3. The fitting curves for (a) PAMPSA-GO, (b) PAA-GO, (c) PHEA-GO, (d) PPEG-GO, (e) PDMA-GO, (f) PAM-GO, and (g) PAETAC-GO in their Raman spectrum, and the pink and light blue peaks correspond to free and intermediate water, respectively. The inset figures are the schematic illustration of the water molecule configuration. (h) The IW:(IW+FW) ratios of all the hydrogels calculated from their Raman spectrum in the O-H stretching energy area. (i) The equivalent water vaporization enthalpy of the water in the hydrogels, the green enthalpy drop represents for the enthalpy reduced by the interaction between the water molecules and corresponding hydrophilic group.

absorbed too much FW, resulting in increased heat loss to the bulk water, and thus higher bulk water temperatures. The mass loss of hydrogels was recorded using a mass balance. As shown in Figure 4d, the vapor generation rates of all the hydrogel-based SVGs were significantly quicker than that of pure water. These evaporation rates were also in good agreement with their corresponding intermediate water content and equivalent water vaporization enthalpies. PAMPSA-GO and PAETAC-GO presented much lower evaporation rates than the neutral polymer hydrogels, owing to their lower intermediate water contents, higher heat loss to bulk water, and higher equivalent water vaporization enthalpies. The evaporation rates of neutral hydrogels with the following functional groups can be ranked

from high to low as follows: $-\text{NH}_2 > -\text{N}(\text{CH}_3)_2 > -\text{C}-\text{O}-\text{C}- > -\text{OH} > -\text{COOH} > -\text{SO}_3\text{H} > -\text{N}^+(\text{CH}_3)_3\text{Cl}^-$. Among them, the highest evaporation rate of SVG based on PAM-GO was $3.23 \text{ kg m}^{-2} \text{ h}^{-1}$.

Furthermore, the solar-to-vapor energy conversion efficiency of SVG systems were calculated by equation (2):

$$\eta = \frac{\bar{m} \times h_v}{C_{opt} \times P} \quad \text{Eq. (2)}$$

where \bar{m} , h_v , C_{opt} and P refer to the mass flow of evaporation, the absorbed water's equivalent water vaporization enthalpy in the hydrogel, the optical intensity, and the power of sun irradiation, respectively. The energy efficiency of the PAM-GO based SVG is 94.1 %.

ARTICLE

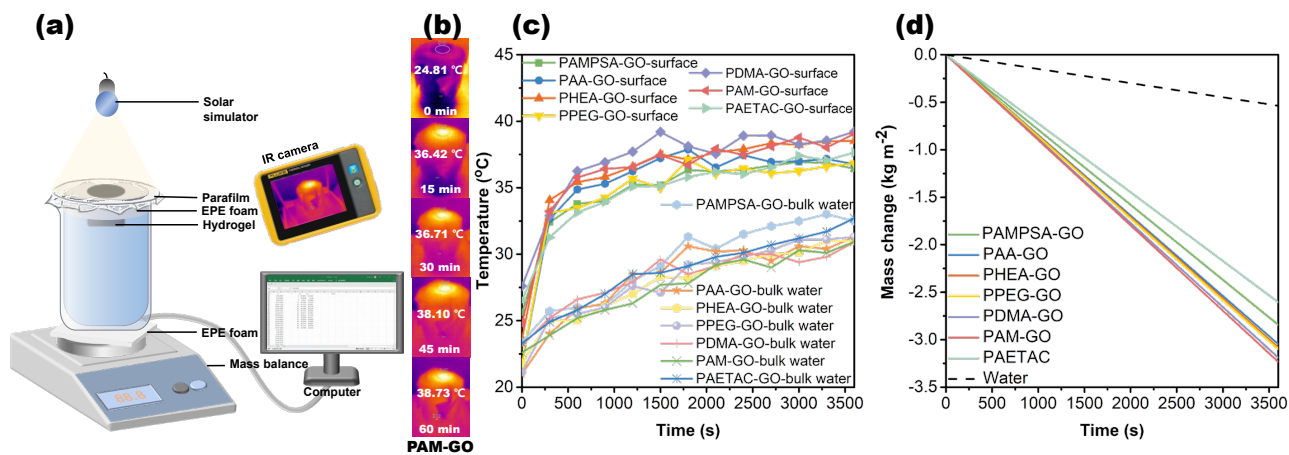


Figure 4. (a) Schematic illustration of the SVG setup. (b) The infrared images of the PAM-GO at the 0 minute, 15 minutes, 30 minutes, 45 minutes and 60 minutes during the SVG testing. (c) The surface temperatures and bulk water temperatures of the hydrogels calculated from the infrared images during one-hour SVG testing under one sun. (d) Water mass loss of the hydrogels and pure water under one sun. Notably, all of the data were calibrated with dark evaporation data.

Overall, the structure-property-application relationships of the hydrogel-based SVG have been illustrated in Table 1. The differences in the chemical structure of hydrogels are mainly reflected in the diverse hydrophilic functional groups contained in the repeating units, which can arouse distinct interactions with the BW molecules and hence IW. The groups with high potentials such as $-\text{SO}_3\text{H}$ and $-\text{N}^+(\text{CH}_3)_3\text{Cl}^-$ groups can establish strong interaction with the water molecules, as evidenced by the high energy that IW required to overcome the hydrogen bonding, the massive quantities of FW, and the high equivalent water evaporation enthalpy. As a result, the corresponding PAMPSA-GO and PAETAC-GO SVGs showed lower evaporation rates than that of other neutral polymer hydrogels. They are able to establish mild interaction with the water molecules, which

Table 1. Structure-property-application relationships of the polymeric hydrogels.

Sample name	Chemical structure	E_{hyd} (kJ mol ⁻¹)	IW:(IW+FW)	h_v (J g ⁻¹)	Evaporation rate (kg m ⁻² h ⁻¹)
PAETAC-GO		26.78	0.538	1838.79	2.61±0.27
PAMPSA-GO		23.94	0.559	1758.07	2.84±0.11
PAA-GO		17.17	0.579	1343.83	3.05±0.13
PHEA-GO		12.51	0.585	1200.34	3.08±0.12
PPEG-GO		9.64	0.635	1111.64	3.10±0.10
PDMA-GO		8.96	0.757	1066.66	3.19±0.04
PAM-GO		6.68	0.782	1047.56	3.23±0.04

is reflected in the fact that IWs are more readily released from hydrogen bonds. The higher content as well as the easier vaporization of the IW can guarantee lower equivalent water vaporization enthalpy and better SVG performance. Hydrophilic groups in our study can be rated as follows in terms of their potential for SVG application: $-\text{N}^+(\text{CH}_3)_3\text{Cl}^- < -\text{SO}_3\text{H} < -\text{COOH} < -\text{OH} < -\text{C}-\text{O}-\text{C}- < -\text{N}(\text{CH}_3)_2 < -\text{NH}_2$, giving a guideline for the selection of raw materials in the fabrication of the hydrogel SVGs.

Finally, the hierarchical porous PAM-GO SVG with pendant amino groups, which stands out from the other six hydrogels, has been applied in seawater desalination (Figure 5). The seawater used for desalination was obtained from Darling Harbour (Sydney, Australia; E151.20°, S33.87°) with a total dissolved solids of 36.2 g L⁻¹. The PAM-GO has been set in a container same as Figure 4a but full of seawater for half a month and was taken to conduct a three-hours continuous SVG test everyday (Figure 5a). It can maintain its evaporation rate during the fifteen times of repetition, and could reach a high average rate of 3.41 kg m⁻² h⁻¹, showing good durability in seawater. No appreciable salt accumulation was seen on the hydrogel's surface after daily desalination, indicating good salt resistance. This could be attributed to the hydrogel's rapid water replenishment capability, which impede rapid concentration decline at the evaporation surface and super-saturation of salt solutions.⁴⁵ In addition, the evaporation rates of other hydrogels in seawater desalination followed the similar trend as that in DI water (Figure S5). For further analyse the desalination effect, we employed a sealed jar with glass cover to collect the condensed water (Figure 5b). After longtime desalination, the condensed water in the jar was collected for ICP-MS analysis (Figure 5c) and total dissolved solids measurement (Figure 5d). Compared to the untreated seawater, the concentrations of the four principal ions (Na^+ , Mg^{2+} , K^+ and Ca^{2+}) and the total

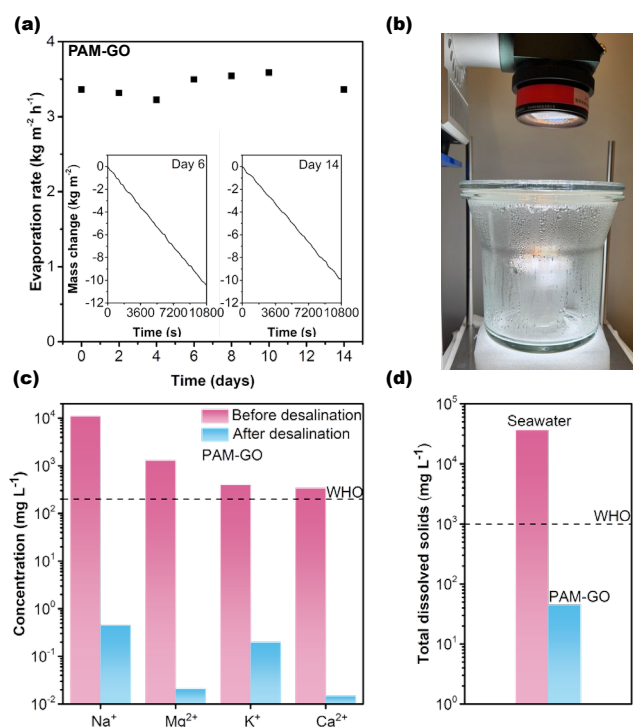


Figure 5. PAM-GO hydrogel based SVG desalination performance. (a) The evaporation rates of PAM-GO after being exposed to seawater for different days in 15 days. Inset: Solar vapor generation performance after one and two weeks of exposure to seawater. (b) The sealed jar for the condensed water collection. (c) The four primary ion concentrations of the seawater and the condensed water. (d) The total dissolved solids of the seawater and the condensed water.

dissolved solids in the condensed water have been lowered by three to five orders of magnitude, and of course are lower than the World Health Organization (WHO) recommended levels for drinking water.⁴⁶⁻⁴⁹

Conclusion

In this study, we prepared a series of hydrogels for SVG application. The highly charged polymeric hydrogels with $-\text{SO}_3\text{H}$ or $-\text{N}^+(\text{CH}_3)_3\text{Cl}^-$ groups showed relatively poor SVG performance due to their high FW absorption ratio as well as strong interaction with water molecules. In contrast, the hierarchical porous PAM-based SVG exhibits excellent water evaporation rate and outstanding durability and desalination capability. To discover the structure-property-application relationships of hydrogel SVG, we investigated the interactions between polymer chains and water molecules in detail, studied swelling ratio and water replenishment capability, calculated the IW contents and evaporation enthalpies, and fairly compared their SVG performance. Our study shows that under the same experimental conditions, hydrophilic hydrogels can be ranked as follows in terms of their potential for SVG application: $-\text{N}^+(\text{CH}_3)_3\text{Cl}^- < -\text{SO}_3\text{H} < -\text{COOH} < -\text{OH} < -\text{C}-\text{O}-\text{C}- < -\text{N}(\text{CH}_3)_2 < -\text{NH}_2$. We thus believe that

our study could fill the knowledge gap in hydrogel SVGs and promote the development of next generation SVG technology.

Experimental section

Materials

Chemicals involving 2-acrylamido-2-methyl-1-propanesulfonic acid (AMPSA), acrylic acid (AA, 99 wt% in DI water), 2-hydroxyethyl acrylate (HEA, 96 wt% in DI water), poly(ethylene glycol) diacrylate (PEGDA, average $M_n = 575 \text{ g mol}^{-1}$), N,N-dimethylacrylamide (DMA, 99 wt% in DI water), acrylamide (AM), [2-(acryloyloxy)ethyl]trimethylammonium chloride (AETAC, 80 wt% in DI water), graphene oxide (GO, powder, 15-20 nanosheets, 4-10% edge-oxidized), N,N'-methylenebis(acrylamide) (MBI), ammonium persulfate (APS), L-Ascorbic acid (Vitamin C, VC), N,N,N',N'-tetramethyl-ethylenediamine (TEMED), were all utilized without any further purification after being acquired from Sigma-Aldrich Australia.

Synthesis of hydrogels in acid condition

As the mixture of acidic monomer (AMPSA or AA), cross-linker and GO solution is in an acid condition, Vitamin C served as the catalyst. Typically, 277.11 mg of AMPSA was mixed with 22.89 mg of MBI, 36 mg of VC and 1.9 mL of GO solution (1.5 mg mL^{-1} in DI water) by sociation. Following that, to start the gelation, 0.1 mL of APS solution (0.3 g mL^{-1} in DI water) was added and stirred. The synthesised gel was triple-washed with DI water after being frozen overnight at $-18 \text{ }^\circ\text{C}$ and thawed in DI water at room temperature to obtain a pure PAMPSA-GO hydrogel. Similar steps were followed for generating PAA-GO hydrogel, with the exception of the amounts of AA (242.43 mg, 99 wt% in DI water) and MBI (57.57 mg). Before being characterised, all of the hydrogels were freeze-dried. And prior to the solar vapor generation tests, they were all well-saturated in DI water or seawater.

Synthetic procedure for other hydrogels

For the other neutral or alkaline monomers, TEMED worked as the catalyst. Typically, 261.48 mg of HEA was mixed with 38.49 mg of MBI, 10 μL of TEMED and 1.9 mL of GO solution (1.5 mg mL^{-1} in DI water) by sociation. Following that, to start the gelation, 0.1 mL of APS solution (0.3 g mL^{-1} in DI water) was added and stirred. The synthesised gel was triple-washed with DI water after being frozen overnight at $-18 \text{ }^\circ\text{C}$ and thawed in DI water at room temperature to obtain a pure PHEA-GO hydrogel. Similar steps were followed for generating PPEG-GO, PDMA-GO, PAM-GO, PAETAC-GO hydrogels, with the exception of the amounts of monomers and MBI (listed in Table S2). Before being characterised, all of the hydrogels were freeze-dried. And prior to the solar vapor generation tests, they were all well-saturated in DI water or seawater.

Characterizations

Malvern 2000 particle size analyzer (Malvern, United Kingdom) was used to confirm the zeta potential of the polymers. With the help of a Zeiss scanning electron microscope (SEM) (10–30 kV), the hydrogels' pore structure was explored. By using a Shimadzu MIRacle 10 FT-IR, Fourier transform infrared spectroscopy (FT-IR) results were obtained.

Using a Shimadzu 1700 UV-visible-NIR spectrophotometer operating in the wavelength range of 300-2500 nm, UV-vis-NIR absorbance spectra were gathered. A Renishaw Raman spectroscopy was used to acquire the Raman spectra. A Q600 SDT Thermal Analyser (DSC-TGA) was used to track the heat change of hydrogels from room temperature to 200 °C at a heating rate of 10 °C min⁻¹. Using an Agilent 7900 ICP-MS, the principal four ion concentrations in seawater and desalinated water were examined. A portable multimeter called the HQ40D was used to measure the total dissolved solids (TDS) in both seawater and desalinated water.

Simulation study

The simulation study was conducted based on Merck Molecular Force Field 94 (mmff94) using *Avogadro* software.

Solar vapor generation tests

To simulate the sun irradiation, a solar simulator (NBeT HSX-F3000 xenon light source) was utilized. The solar irradiance on the gel surface was calibrate to one sun (1 kW m⁻²) by a portable power and energy metre console with a thermal power sensor (PM100D and S405C, Thorlabs, Germany). The testing hydrogel was fixed in the middle of a floating EPE foam on the top of a beaker full of DI water or seawater. To avoid the potential effects of bulk water evaporation, a parafilm was employed to fill a few small areas between the EPE foam and the beaker. During the SVG testing, the water mass losses over time were recorded by an electronic mass balance (OHAUS Pioneer IC-PX 124). In order to insulate the heat transferred between the mass balance and the beaker, another EPE foam was also placed between them. The slopes of the mass loss-time curve were calculated using linear fitting to determine the evaporation rates. During the solar vapor generation tests, the temperatures of the hydrogel surface and the bulk water were measured every five minutes using a Fluke PTi120 pocket thermal imager.

Conflicts of interest

The authors declare no competing financial interest.

Acknowledgements

Qiang Fu acknowledges the Australian Research Council under the Future Fellowship (FT180100312). Shudi Mao acknowledges the support from the China Scholarship Council (CSC) Scholarship (202006140015).

References

1. S. Kalogirou, *Progress in Energy and Combustion Science*, 2005, **31**, 242-281.
2. D. N. Chakkaravarthy, *International Journal of Agriculture Environment and Biotechnology*, 2019, **12**, 187-193.
3. W. W. Immerzeel, L. P. Van Beek and M. F. Bierkens, *Science*, 2010, **328**, 1382-1385.
4. A. Panagopoulos, K.-J. Haralambous and M. Loizidou, *Science of The Total Environment*, 2019, **693**, 133545.
5. R. Semiat, *Environmental science & technology*, 2008, **42**, 8193-8201.
6. A. D. Khawaji, I. K. Kutubkhanah and J.-M. Wie, *Desalination*, 2008, **221**, 47-69.
7. F. A. AlMarzooqi, A. A. Al Ghaferi, I. Saadat and N. Hilal, *Desalination*, 2014, **342**, 3-15.
8. M. A. Shannon, P. W. Bohn, M. Elimelech, J. G. Georgiadis, B. J. Marinas and A. M. Mayes, *Nature*, 2008, **452**, 301-310.
9. Z. Deng, J. Zhou, L. Miao, C. Liu, Y. Peng, L. Sun and S. Tanemura, *Journal of Materials Chemistry A*, 2017, **5**, 7691-7709.
10. O. Neumann, A. S. Urban, J. Day, S. Lal, P. Nordlander and N. Halas, *ACS nano*, 2013, **7**, 42-49.
11. S. Ma, C. P. Chiu, Y. Zhu, C. Y. Tang, H. Long, W. Qarony, X. Zhao, X. Zhang, W. H. Lo and Y. H. Tsang, *Applied energy*, 2017, **206**, 63-69.
12. Z. Zhu, Y. Xu, Y. Luo, W. Wang and X. Chen, *Journal of Materials Chemistry A*, 2021, **9**, 702-726.
13. Z. Xu, Z. Li, Y. Jiang, G. Xu, M. Zhu, W.-C. Law, K.-T. Yong, Y. Wang, C. Yang, B. Dong and F. Xing, *Journal of Materials Chemistry A*, 2020, **8**, 25571.
14. Z. Xie, J. Zhu and L. Zhang, *ACS Appl Mater Interfaces*, 2021, **13**, 9027-9035.
15. P. Zhang, Q. Liao, H. Yao, H. Cheng, Y. Huang, C. Yang, L. Jiang and L. Qu, *Journal of Materials Chemistry A*, 2018, **6**, 15303-15309.
16. F. Gong, H. Li, W. Wang, J. Huang, D. Xia, J. Liao, M. Wu and D. V. Papavassiliou, *Nano Energy*, 2019, **58**, 322-330.
17. P.-F. Liu, L. Miao, Z. Deng, J. Zhou, H. Su, L. Sun, S. Tanemura, W. Cao, F. Jiang and L.-D. Zhao, *Materials Today Energy*, 2018, **8**, 166-173.
18. H. Su, J. Zhou, L. Miao, J. Shi, Y. Gu, P. Wang, Y. Tian, X. Mu, A. Wei, L. Huang, S. Chen and Z. Deng, *Sustainable Materials and Technologies*, 2019, **20**, e00095.
19. W. Li, X. Li, W. Chang, J. Wu, P. Liu, J. Wang, X. Yao and Z.-Z. Yu, *Nano Research*, 2020, **13**, 3048-3056.
20. T. Yang, H. Lin, K.-T. Lin and B. Jia, *Sustainable materials technologies*, 2020, **25**, e00182.
21. Y. Wang, J. Zhang, W. Liang, H. Yang, T. Guan, B. Zhao, Y. Sun, L. Chi and L. Jiang, *CCS Chemistry*, 2021, **4**, 1153-1168.
22. I. Ibrahim, D. H. Seo, A. M. McDonagh, H. K. Shon and L. Tijjing, *Desalination*, 2021, **500**, 114853.
23. T. Li, Q. Fang, J. Wang, H. Lin, Q. Han, P. Wang and F. Liu, *Journal of Materials Chemistry A*, 2021, **9**, 390-399.
24. J. Chen, M. Lee, Y. Qiu, C. Wu, B. Li and Y. Yin, *SmartMat*, 2022, **4**, e1140.
25. Y. Guo, X. Zhou, F. Zhao, J. Bae, B. Rosenberger and G. Yu, *ACS Nano*, 2019, **13**, 7913-7919.
26. X. Zhou, F. Zhao, Y. Guo, B. Rosenberger and G. Yu, *Science Advances*, 2019, **5**, eaaw5484.
27. B. Yang, Z. Zhang, P. Liu, X. Fu, J. Wang, Y. Cao, R. Tang, X. Du, W. Chen, S. Li, H. Yan, Z. Li, X. Zhao, G. Qin, X. Q. Chen and L. Zuo, *Nature*, 2023, DOI: 10.1038/s41586-023-06509-3.
28. F. Zhao, X. Zhou, Y. Shi, X. Qian, M. Alexander, X. Zhao, S. Mendez, R. Yang, L. Qu and G. Yu, *Nat Nanotechnol*, 2018, **13**, 489-495.
29. X. Zhou, F. Zhao, Y. Guo, Y. Zhang and G. Yu, *Energy & Environmental Science*, 2018, **11**, 1985-1992.
30. S. Mao, M. Johir, C. Onggowarsito, A. Feng, L. Nghiem and Q. Fu, *Materials Advances*, 2022, **3**, 1322-1340.

31. F. Zhao, Y. Guo, X. Zhou, W. Shi and G. Yu, *Nature Reviews Materials*, 2020, **5**, 388-401.
32. X. Zhou, Y. Guo, F. Zhao and G. Yu, *Acc Chem Res*, 2019, **52**, 3244-3253.
33. C. Onggowarsito, A. Feng, S. Mao, S. Zhang, I. Ibrahim, L. Tijjing, Q. Fu and H. H. Ngo, *Environmental Functional Materials*, 2022, **1**, 196-203.
34. C. Onggowarsito, A. Feng, S. Mao, L. N. Nguyen, J. Xu and Q. Fu, *ChemSusChem*, 2022, **15**, e202201543.
35. Q. Zhao, Z. Huang, Y. Wan, J. Tan, C. Cao, S. Li and C.-S. Lee, *Journal of Materials Chemistry A*, 2021, **9**, 2104-2110.
36. X. Zhou, Y. Guo, F. Zhao, W. Shi and G. Yu, *Adv Mater*, 2020, **32**, 2007012.
37. M. Yang, H. Luo, W. Zou, Y. Liu, J. Xu, J. Guo, J. Xu and N. Zhao, *ACS Appl Mater Interfaces*, 2022, **14**, 24766-24774.
38. Y. Zhou, T. Ding, M. Gao, K. H. Chan, Y. Cheng, J. He and G. W. Ho, *Nano Energy*, 2020, **77**, 105102.
39. C. Liu, Y. Peng and X. Zhao, *Desalination*, 2021, **501**, 114911.
40. X. Zheng, Y. Bao, A. Huang, G. Qin and M. He, *Separation and Purification Technology*, 2023, **306**, 122741.
41. S. Mao, C. Onggowarsito, A. Feng, S. Zhang, Q. Fu and L. D. Nghiem, *Journal of Materials Chemistry A*, 2023, **11**, 858-867.
42. Y. Guo, L. S. de Vasconcelos, N. Manohar, J. Geng, K. P. Johnston and G. Yu, *Angewandte Chemie International Edition*, 2022, **134**, e202114074.
43. C. Li, L. Fan, R. Zhu, X. Li, P. Wen, X. Zhao, G. Wang, J. Zou and F. Kim, *ACS Applied Energy Materials*, 2020, **3**, 9216-9225.
44. F. H. Isikgor, A. S. Subbiah, M. K. Eswaran, C. T. Howells, A. Babayigit, M. De Bastiani, E. Yengel, J. Liu, F. Furlan and G. Harrison, *Nano Energy*, 2021, **81**, 105633.
45. S.-L. Loo, L. Vásquez, M. Zahid, F. Costantino, A. Athanassiou and D. Fragouli, *ACS Applied Materials and Interfaces*, 2021, **13**, 30542-30555.
46. W. H. Organization, *Potassium in drinking-water: background document for development of WHO guidelines for drinking-water quality*, World Health Organization, 2009.
47. W. H. Organization, *Calcium and magnesium in drinking water: public health significance*, World Health Organization, 2009.
48. G. WHO, *World health organization*, 2011, **216**, 303-304.
49. W. H. Organization, *Guidelines for drinking-water quality*, World Health Organization, 2004.